

# CFD INVESTIGATION ON FLOW AND HEAT TRANSFER FOR AN ADVANCED SHROUDED ROTOR TIP CONCEPT

*F. Cottier – E. Lutum*

MTU Aero Engines GmbH, Dachauer Str. 665, 80995 München, Germany,  
francois.cottier@mtu.de – ewald.lutum@mtu.de

## ABSTRACT

Aerothermal investigations to study flow and heat transfer of a high pressure turbine rotor blade were carried out to analyse the coolant effect in the shroud area. The purpose of these investigations is to improve the physical understanding of the flow and the thermal effects in the shroud region, mainly between the fins.

The investigation will focus on film cooling effectiveness and heat transfer coefficient in the shroud region, between the fins (top surface), on the blade platform (bottom surface) and on the blade surface. Different cooling mass flow rates were imposed from the stator shroud (0%, 0.75% and 1.5% coolant ratio). A general objective is to improve the calibration and validation of CFD models (ANSYS CFX) for design purposes, based on experimental data. Computations were performed using a small temperature difference of 5 K and a larger temperature difference of 30 K between the main and coolant flow. Additionally computations using a “tracer” have been conducted, making use of the heat and mass analogy. The predictions using the larger temperature difference and the “tracer” method showed good agreement with film cooling effectiveness values derived from measurements. In contrast, predictions using the small temperature difference indicated poor agreement with these measurements. Predicted heat transfer results show good agreement with measured data on the bottom shroud (bottom surface) surface. However, significant under prediction of heat transfer levels was found for the top shroud region.

The investigations involved also an evaluation of the numerical modelling of the rotor-stator interface, comparing a mixing plane with different steady state "frozen rotor" stator to rotor positions.

## NOMENCLATURE

$C_R$	-	Coolant ratio ( $= \dot{m}_c / \dot{m}_\infty$ )
$C$	-	Concentration
$h$	$W/(m^2K)$	Heat transfer coefficient
$\dot{m}$	$kg/s$	Mass flow
$q$	$W/m^2$	Wall heat flux
$Re$	-	Reynolds number
$T$	$K$	Total temperature
$y^+$	-	Near-wall coordinate in wall-normal direction
Greek symbols		
$\theta$	-	Dimensionless temperature ratio
$\eta$	-	Film cooling effectiveness
$\phi$	-	Flow coefficient (Axial flow velocity/Blade speed at mid span)
Subscripts		
aw		Adiabatic Wall
iw		Impermeable wall condition
$\infty$		Main flow inlet value
LE		Leading edge
SS		Suction side

TE	Trailing edge
w	Wall
C	Coolant inlet value
L	Local value

## INTRODUCTION

Less fuel, less exhaust emission, less noise, high performance, low maintenance: the requirements on aero engines are continuously rising. High oil and kerosene prices as well as tight noise and emission restrictions at many airports demand for higher efficiency. Also environmental aspects as global warming or the shortage of natural resources require improvements and new technologies to minimize those problems. Since the turbine inlet temperature is a main parameter to reduce the specific fuel consumption the inlet temperatures are rising continuously to increase the efficiency of the overall engine. Therefore, high inlet temperatures also raise new requirements on the blade material and cooling systems. Since nowadays the HP turbine inlet temperatures are above 1600°C, complex cooling methods are necessary to cool the blade to a material endurable temperature. It is therefore of great interest to study the cooling effect in the shroud area, which is a sensitive part of the blade. The cooling of turbine blade shrouds has become a necessity. Active shroud cooling, i.e. by means of internal cooling passages in the shroud is effective but requires thick, heavy and expensive shrouds. Passive shroud cooling, on the other hand, reduces the driving gas temperatures by ejecting coolant from stationary parts making use of local 3D flow structures to transport the coolant to where it is needed. Concerning passive shroud cooling concepts that are already in engine applications, research now focuses on a detailed understanding of the flow physics and a better assessment of the cooling effectiveness and the aerodynamic penalties combined with such a cooling concept. In the last years many efforts have been carried out to understand and better predict the flow and the heat transfer in the shrouded blade cavities and on the interaction with the main flow path. It is shown by Porreca et al. [1], Lampart et al. [2], Nirmalan and Bailey [3] and Giboni et al. [4] that the secondary flow in the main passage is largely influenced by the cavity flow. The interaction is observed up to blade mid span and the secondary flow is mainly influenced by the mass flow and the direction of the leakage. Porreca et al. [1] stress that the gain can be up to one point in the overall stage efficiency using an optimized shrouded blade geometry. Since the global performance of the turbine is highly influenced by the tip leakage, the geometry of the shrouded cavity has a large effect on the flow field as Nirmalan and Bailey [3] show. The clearance gap as well as the geometry itself of the shroud (scalloped or non-scalloped) plays a significant role, i.e. larger clearance gap increases losses. Bohn et al. [5] investigated the axial gap between the shroud and the endwall (open and closed cavities) and stress that a large gap displaced the secondary flow in the main flow path. Locally on the shroud area it is also shown that the geometry has an effect on the cooling efficiency. Nirmalan et al. [6] shows that the cooling effect decreases when the gap increases and also mentioned the effect of the rotation in the results. Haller and Hilditch [7] carried out heat transfer investigations at blade shroud bottom and top surfaces. The authors stress the influence of the laminar-turbulent transition on the heat transfer coefficient distribution on the bottom part and of the tangential shroud gaps.

Recently Kanjirakkad [9] investigated passive shroud cooling concepts to avoid thick shrouds with active internal and film cooling. An improved through-platform cooling concept was derived which has superior aerodynamic and cooling performance compared to conventional cooling methods. A subsequent experimental study of the above mentioned advanced through platform cooling concept was conducted by Lehmann et al. [11] in a low speed large-scale turbine rig to obtain detailed investigated flow field and convective heat transfer measurements in the shroud region of a high pressure turbine blade.

The present investigation is part of the European research project AITEB-2 (Aerothermal investigations of turbine endwalls and blades) that aims at optimizing cooling configurations at highly loaded turbine blades (Janke and Wolf [8]). A comparison between experimental and CFD

results is performed to evaluate the capability of CFD to simulate the mixing between cooling and main flow and heat transfer mainly in the shroud area.

## GEOMETRY AND SETUP OF SIMULATIONS

The present investigations are linked to the experiments conducted by Lehmann et al. [11]. This experimental facility consisted of a turbine stage with 26 stator and 45 rotor blades. Each rotor blade carried a shroud with three forward leaning fins. Inter-shroud gaps of 1.3mm width separated the individual rotor shrouds in the circumferential direction. The rotor casing above the shroud consisted of a parallel annulus with a backward facing step between the first and second fin. The current shroud cooling configuration is shown in Fig.1. The coolant air was supplied to a plenum outside the stator casing by a secondary air system. It was ejected through 260 circular holes in the stator platform overhang downstream of the stator trailing edge at a tangential angle of  $+65^\circ$  relative to axial direction and a radial angle of  $30^\circ$  relative to platform surface.

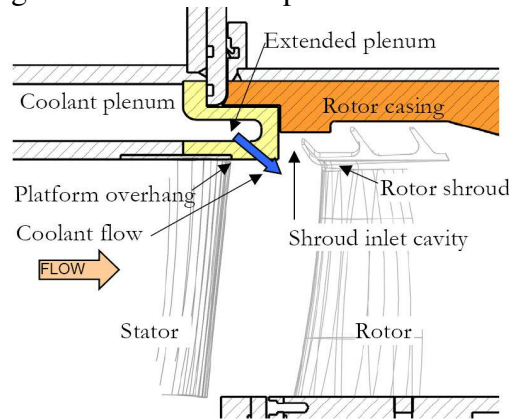


**Fig. 1 : Passive shroud cooling configuration (Kanjirakkad [9])**

With respect to the geometry used in simulations a discretisation of the entire turbine would result in either a very coarse mesh at an acceptable size or a huge mesh size, which would require very high computer resources. Hence, in simulations the discretisation domain was minimized due to periodicity conditions. The CFD model consisted of two separate domains, i.e. stator and rotor, connected by a rotor-stator interface. In the static part of the domain the cavity was modelled, which simulated the inlet for the cooling flow. The CFD boundary conditions are representative of the experimental setup. The boundary conditions shown in the Tab. 1 show the 3 cooling ratios studied for one general working point. The boundary conditions at inlet and outlet have been kept constant in order to compare the influence of the coolant mass flow rate.

		$Re=500000, \phi=0.42, C_R=0.0\% ; 0.75\% ; 1.5\%$			
		Inlet	Exit	Coolant case I	Coolant case II
flow angle	$^\circ$	0.0			
rotational speed	rpm	359			
pressure, total	Pa	99419.2			
pressure, static	Pa		98324.5		
temperature, total	K	279.20		283.58 ( $\Delta T \sim 5$ K)	308.58 ( $\Delta T \sim 30$ K)
mass flow	kg/s			0 ; 0.0025 ; 0.0051	
turbulence intensity	-	1.0%			
viscosity ratio	-	10.00			

**Tab. 1: Investigated boundary conditions**

## Grid generation

The quality of the results of a CFD calculation may strongly depend on the used grid. Therefore, one of the main parts of a CFD investigation is the development of a well adapted grid concerning

the geometry and the physical problem to ensure that the solution computed depends only on the numerical model and is independent of the grid.

The mesh used for the following investigations is a hybrid mesh generated by ALSTOM as part of a common mesh study in the AITEB consortium. The general mesh statistics are summarised in Tab. 2. A well resolved boundary layer resolution was established by using hexahedral layers close to the walls to enable a low-Reynolds formulation for the near wall treatment. Sufficient refinement of the first cell give  $y^+$  values in the range of 0-2.

Parameter	Stator	Rotor	Total
Total number of nodes	1537373	1459104	2996477
Total number of elements	5309693	5237157	10546850
Min orthogonality angle [degree]	15.2	10.5	10.5
Max aspect ratio	1279.8	1617.6	1617.6
Max element volume ratio	42.4	411.0	411.0

**Tab. 2: Summary of mesh characteristics**

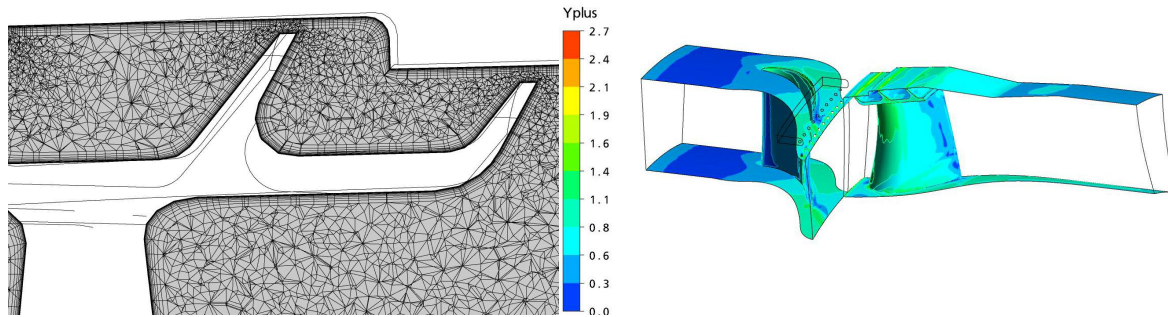


**Fig. 2: Hybrid mesh with hexahedral layers and  $y^+$  surface distribution**

The CFD solver used was the commercial code ANSYS CFX version 11.0 with the Menter SST turbulence model and the Langtry Menter gamma theta transition model (ANSYS-CFX [10]). Automatic wall treatment was applied, which means that the formulation (Low-Reynolds or wall function) depends on the local  $y^+$  value at the wall based on the scalable wall functions. A quasi 2<sup>nd</sup> order spatial discretisation and an automatic time step control was used. The steady state computations were performed with different rotor-stator interface methods, i.e. a general mixing plane stage or a frozen rotor with frozen relative position of the rotor toward the stator. A scaling of the stator exit profile was applied to adjust for differences between vane and blade pitches.

## RESULTS AND DISCUSSION

The main variation studied is the influence of the coolant mass flow rate on the film cooling effectiveness and heat transfer coefficient. To evaluate the role of the stage circumferential-averaging several positions of “frozen rotor” computations have been simulated to be compared with the stage simulations to stress the influence of different rotor-stator positions on the results and on the cooling transport modelling.

The present predictions are validated against experimental data provided by Lehmann et al.[11] and Lehmann et al. [12]. Flow visualisation of leakage flow and cooling effectiveness results were derived by a foreign gas method in that case the Ammonia-Diazo measurements technique. A novel measurement technology for determining heat transfer on shroud surfaces of a rotating high pressure turbine shroud was developed. Further background information on this experimental investigations are given by Lehmann [13].

It appears that the present CFD computation very well predict the flow structures observed in

the corresponding experiments (Lehmann et al. [12]). The dimensionless temperature  $\theta$  and the film cooling efficiency  $\eta$  are characterised by the temperature difference between the coolant and the main flow. Thanks to the heat-mass analogy these parameters could also be expressed by the ratio of foreign gas concentration to coolant supply concentration.

$$\theta = \frac{T_{\infty} - T_L}{T_{\infty} - T_c} = \frac{C_{\infty} - C_L}{C_{\infty} - C_c} \quad \eta = \frac{T_{\infty} - T_{aw}}{T_{\infty} - T_c} = \frac{C_{\infty} - C_{iw}}{C_{\infty} - C_c} \quad (1)$$

Fig. 3 shows dimensionless temperature distributions downstream of the blade shroud for cooling case I, which corresponds to the performed experiments. Predictions for the lower cooling rate of  $Cr=0.75\%$  indicate that the coolant flow seems to be totally mixed with the main flow. Only a very thin radial area is visible in the computations (right), which is in contrast with measurements (left).

It is known that the CFD codes are sensitive to small temperature differences between two media when determining the mixing fraction of these two media. Therefore a second coolant condition (case II) with an increased temperature difference of about 30 K was defined to avoid numerical errors in the temperature diffusion when mixing the main and the cooling flow.

The authors are aware that the density of the coolant flow is influenced by this modification. Hence, additional computations with a “tracer” gas was performed for coolant cases I and II to evaluate the influence of the density ratio. For these computations the different mass fractions of main flow and coolant flow are determined by an additional transport equation, which allows the determination of local mass fraction and also dimensionless temperature and film cooling effectiveness value (eq. 1). The observed results show very small differences between the two cases and led to the conclusion that the impact of the relative small temperature variation of 25 K seemed to be negligible. Fig. 4 shows corresponding results to those shown in Fig. 3 of adiabatic (left, case II) and tracer (right, case I) predictions. The dimensionless temperature distribution downstream of the rotor, i.e. the mixing between coolant and main flow, is very well modelled by both predictions compared to the experimental results (see Fig.3). In addition, evaluating the CFD computations, the difference between the tracer mass fraction and the temperature computed film cooling effectiveness is small. Similar findings are obtained for the greater coolant flow rate of 1.5% (not shown).

This confirms that numerical errors cause the poor results of the adiabatic computation with the lower temperature difference, i.e. large difference with the experimental data mainly the radial cooling was largely underestimated. Hence, all further comparisons with the experiments will be compared to the CFD results with the larger temperature difference (30 K) and with the “tracer” mass fraction. The use of a larger temperature difference as well as the mass-based simulation with a tracer enables an improvement of all the CFD results and stresses some important points that should not be neglected. For such computation the temperature difference between the coolant and the main flow should be large enough to avoid a numerical discrepancy probably due to diffusion in the energy equations. Using the heat-mass analogy can be a solution to avoid this problem without creating an artificial temperature increase. Nevertheless, in the computed case the error due to the temperature increase remains small.

Fig. 5 presents film cooling effectiveness distributions on the blade suction side for relative positions between 70 and 95 % blade span. The agreement with the experiments is good. The tracer computation shows similar results to the film cooling effectiveness. However, the CFD results show a film cooling effectiveness reduction at nearly 60% stream wise, which is not the case in the experiments. The comparison for the 1.5% coolant case (not shown) shows similar results however with a lower radial dissipation of the coolant in CFD than in experiments.

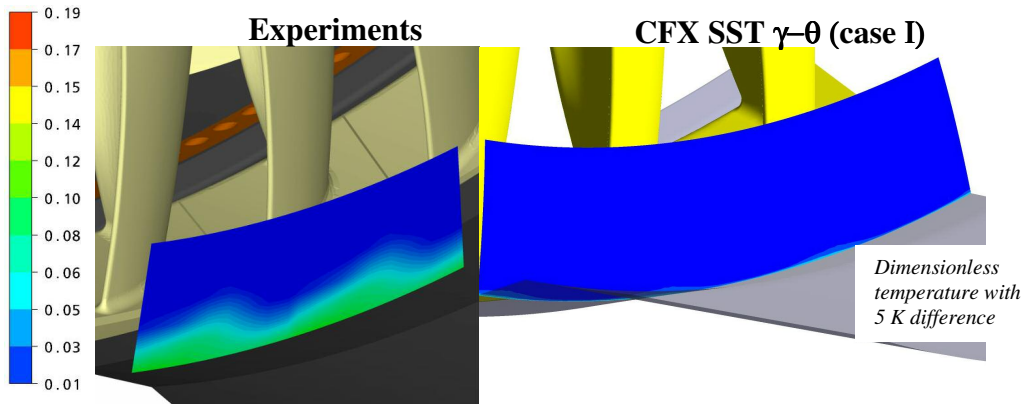


**Fig. 3: Dimensionless temperature distributions downstream of the rotor ( $C_R=0.75\%$ )**

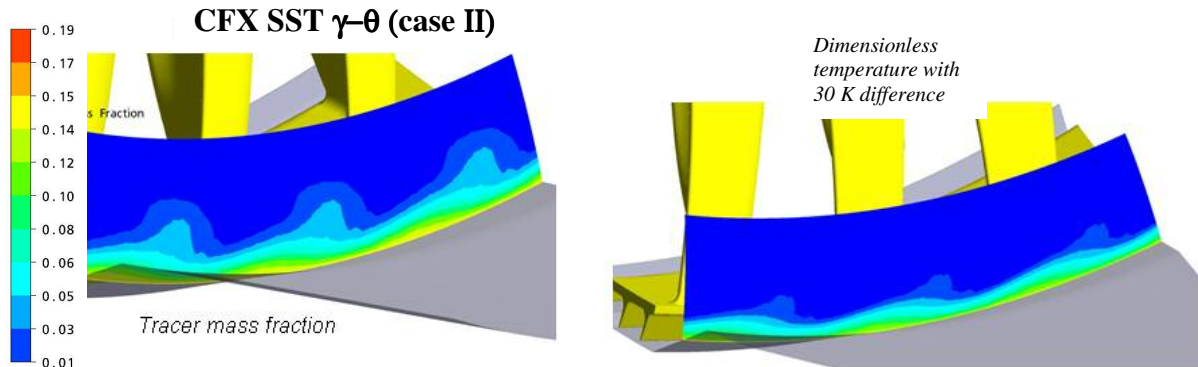


**Fig. 4: Rotor downstream dimensionless temperature ( $C_R=0.75\%$ )**

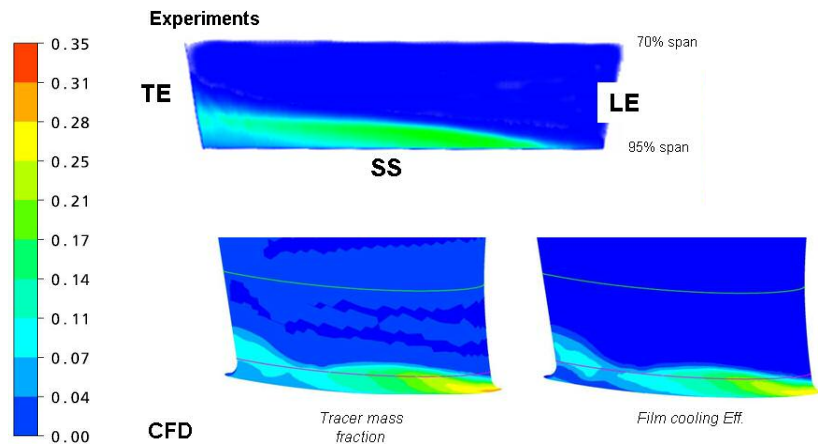


**Fig.5: Film cooling effectiveness (EXP - CFD) and mass fraction (CFD) on the blade suction side ( $C_R=0.75\%$ )**

A comparison of film cooling effectiveness distributions is shown in Fig. 6 for the shroud bottom surface and in Fig. 7 for the shroud top surfaces. Results of adiabatic film cooling effectiveness and tracer mass fraction computations indicate very similar distributions. Both predictions show a good agreement with experiments. Similar observations were found for calculations with a cooling mass flow rate of 1.5 %. (not shown)

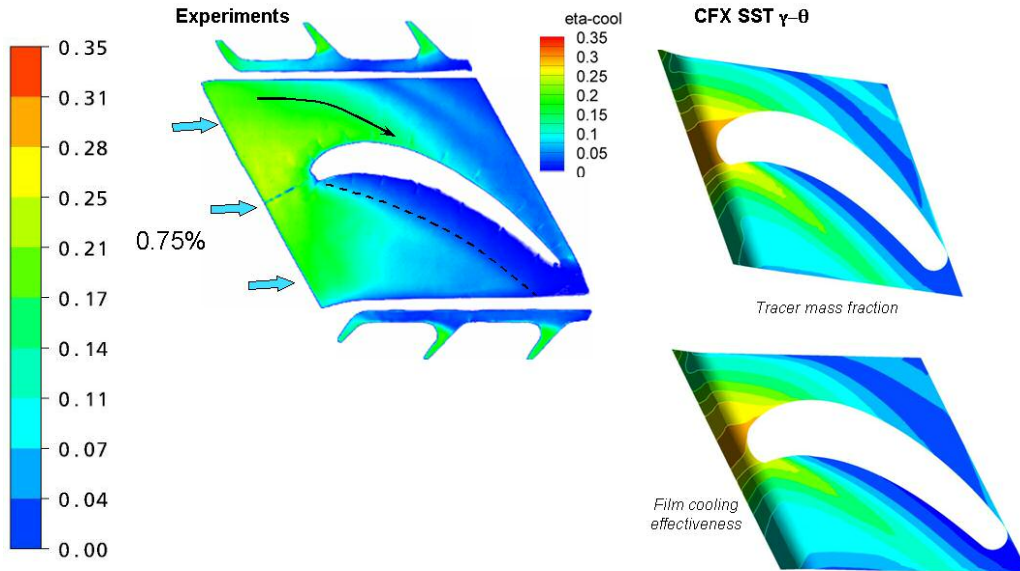


**Fig. 6: Film cooling effectiveness on the shroud bottom surface ( $C_R=0.75\%$ )**

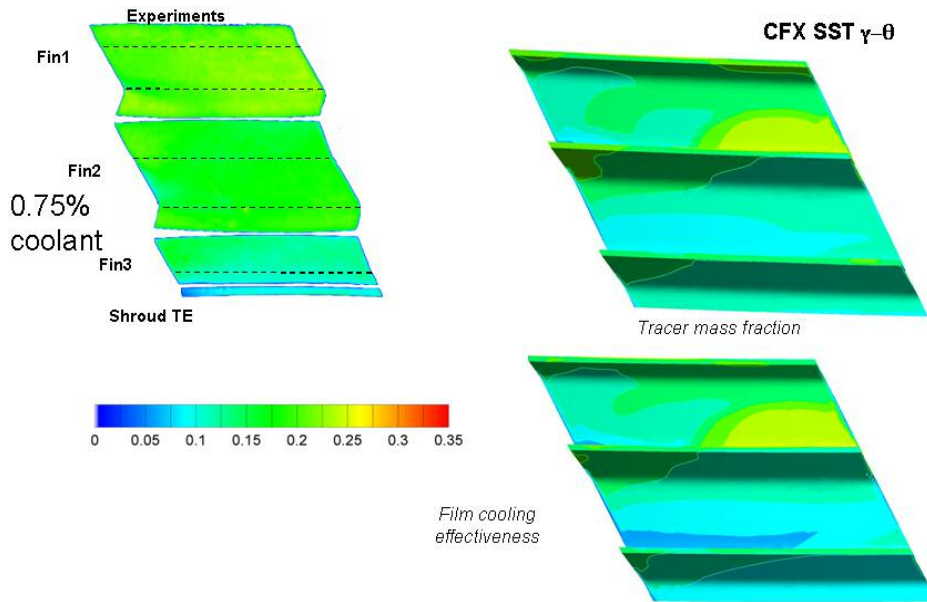


**Fig. 7: Film cooling effectiveness on the shroud top surface ( $C_R=0.75\%$ )**

The heat transfer coefficient is computed with two separate CFD computations. In the first one the wall heat flux is set as boundary conditions (distribution derived from experiments) at the studied walls and the wall temperature  $T_w$  results from the computation. The second one is an adiabatic computation to derive the adiabatic wall temperature  $T_{aw}$  used as reference in the heat transfer coefficient definition.

$$h = \frac{q_w}{T_w - T_{aw}} \quad (2)$$

Current heat transfer predictions are performed for coolant case I conditions and compared with the experimental data by Lehmann et al. [13]. Fig. 8 presents a comparison of heat transfer distributions on the shroud top surface for different coolant mass flow rates. It could be observed from the shown experimental and numerical results that the coolant mass flow rate has only a minor effect on the heat transfer distributions. The comparison between CFD and experiments shows that the predictions underestimate the heat transfer coefficient level by about 50%. However, the local

heat transfer distribution is relatively well simulated.

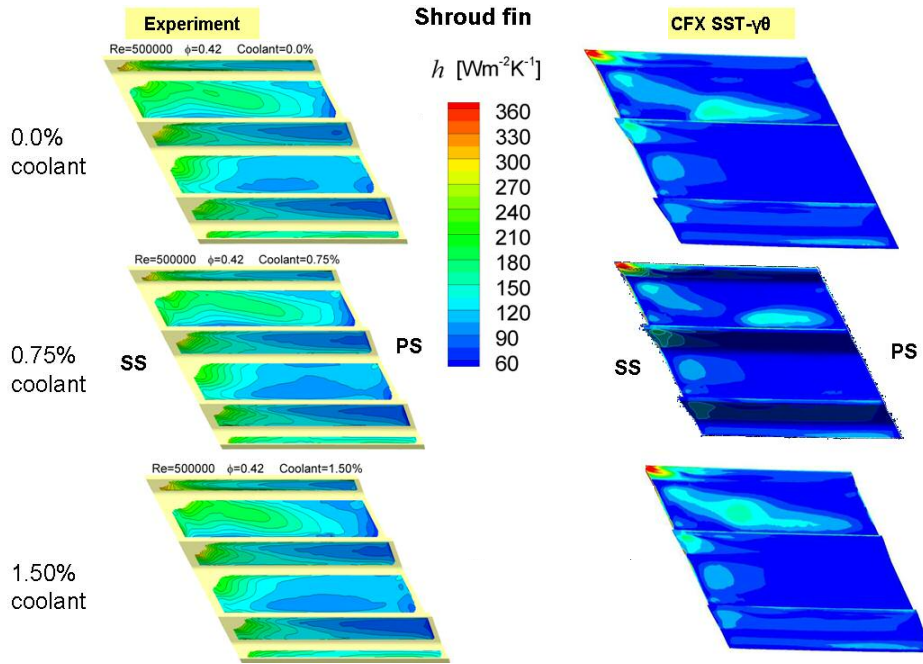


**Fig. 8: Heat transfer coefficient at shroud top surface**

An additional computation with the enlarged temperature difference between the coolant and the main flow was carried out (case II). The predicted heat transfer coefficient was not influenced by the changes. The increase in the reference temperature is counterbalanced by the wall temperature from the computation with heat exchange. This also confirms that the definition of the heat transfer coefficient with the adiabatic wall temperature used as reference enables having a parameter independent of the temperature boundary conditions, as expected.

On the bottom part of the shroud (Fig. 9) experiments are only available for the case without coolant flow. However, the predictions for different cooling flow rates show only a marginal effect on the heat transfer coefficient results. A slight effect is visible over the stagnation areas where the heat transfer coefficient is increased by an increased cooling rate. Generally a good agreement between predictions and experiment is observable on the shroud bottom surface. A slight underestimation of the heat transfer level could be observed.

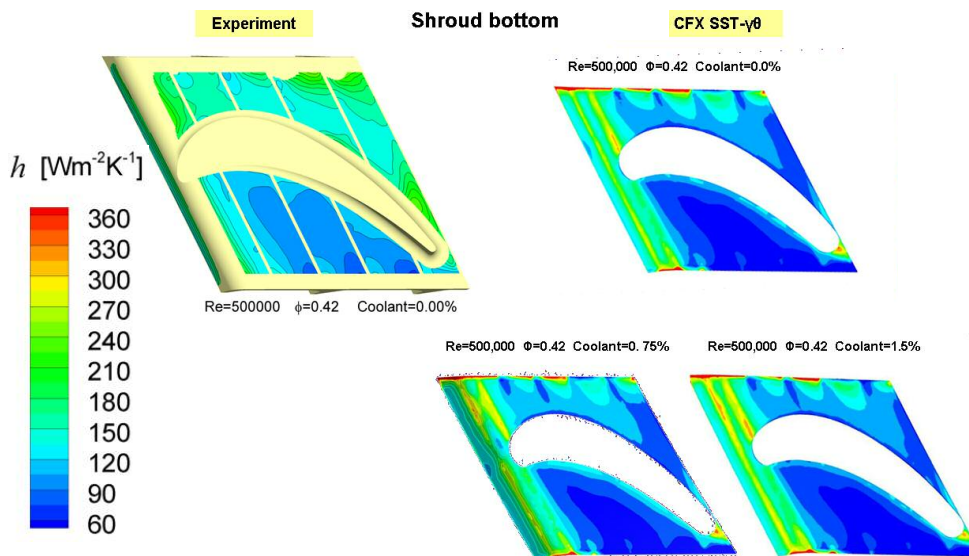


**Fig. 9: Heat transfer coefficient at shroud bottom**

Steady-state computations using a frozen rotor interface between the stator and rotor domains are applied to simulate different relative “frozen” rotor-stator positions. Since the rotor and the stator pitches did not fit adequately the outlet stator profiles need to be scaled to fit with the inlet rotor profiles. Three representative relative rotor-stator positions have been computed and compared with a corresponding stage computation. The reference case will be call  $\Delta=0^\circ$  and relatively to this position two other representative positions are computed, i.e.  $\Delta=4^\circ$  and  $\Delta=7^\circ$ , to achieve different influences of the stator on the rotor. Since this analysis focuses mainly on the differences between stage and the different frozen rotor positions no comparison with experimental results is shown. Tracer mass fraction computations were conducted for coolant case I conditions for a cooling rate of  $C_R=0.75\%$ .

The distributions of film cooling effectiveness on the shroud top surface for stage (upper graph) and different frozen rotor (lower graphs) computations shown in Fig. 10 indicate the sensitivity of the results according relative rotor-stator positions. The stage computation tends to represent an average of the several frozen positions, which can be is quantified by analyzing the average values of the film cooling effectiveness. The two first frozen rotor positions ( $\Delta=0^\circ$  and  $\Delta=4^\circ$ ) present smaller values of film cooling effectiveness ( $\eta_{avg\_ \Delta=0^\circ} = 0.103$  and  $\eta_{avg\_ \Delta=4^\circ} = 0.117$ ) in comparison with the stage prediction ( $\eta_{avg\_stage} = 0.143$ ). Prediction for the frozen rotor position  $\Delta=7^\circ$  indicate greater film cooling effectiveness values ( $\eta_{avg\_ \Delta=7^\circ} = 0.176$ ) compared to the stage results. It is also to be stressed that the axial labyrinth mass flow remains constant within 1.5% for the several cases which implies that the differences are due to local flow effects. To conclude this frozen rotor investigation it is important to say that the thermal parameters and mainly the film cooling effectiveness are sensitive to the relative rotor-stator positions and an unsteady computation could be beneficial. However, the stage computation seems to make a good synthesis of the several investigated positions and may converge to a time-averaged unsteady simulation. That is why it was chosen for time consuming reasons not to carry out any unsteady calculation.

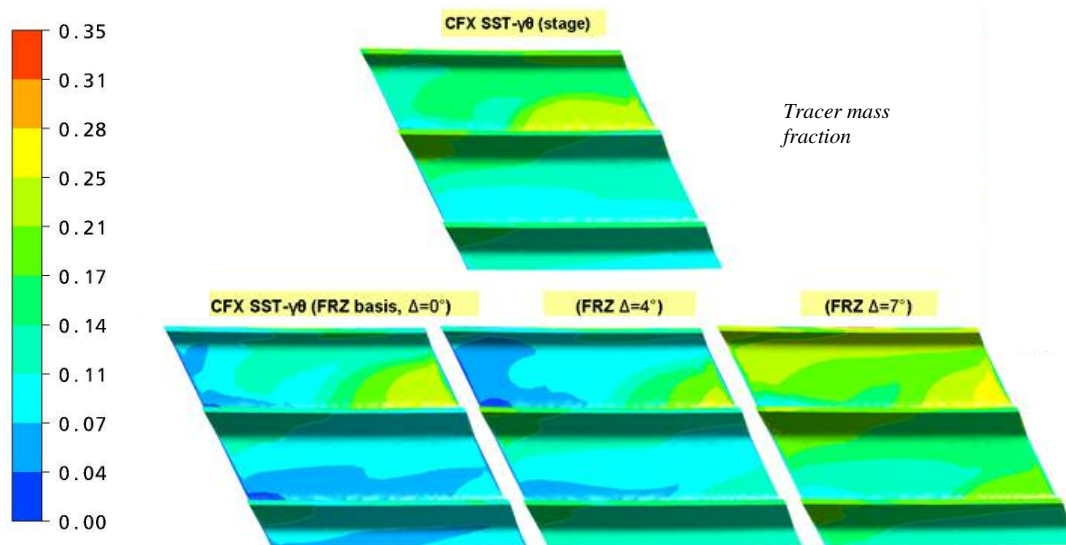


**Fig. 10: Film cooling effectiveness distribution at shroud top surface**

## CONCLUSIONS

CFD computations were conducted for a turbine stage with a flow coefficient of  $\phi=0.42$  and coolant ratios of  $C_R=0\%$ ,  $C_R=0.75\%$  and  $C_R=1.5\%$ . The applied computational hybrid mesh was provided by ALSTOM. Steady state computations were performed with different rotor-stator interfaces, i.e. a general stage mixing plane and a frozen rotor approach.

A main conclusion was that the dimensionless temperature ratio and film cooling effectiveness were highly influenced by the temperature difference between coolant and main flow. A too small

temperature difference (case I) causes numerical errors, which led to incorrect predictions of film cooling effectiveness and dimensionless temperature results. Computations with a sufficient temperature difference (case II) as well as a “tracer” simulation based on the heat-mass analogy indicated good agreement with corresponding measurements. It was further shown that the heat transfer coefficient predictions were not influenced by the temperature boundary conditions. Predictions for both temperature difference cases I and II indicated similar heat transfer results. The predicted heat transfer results compare very well with experimental data on the bottom surface of the blade shroud. by contrast, poor quantitative agreement (off by about 50%) with the experiments was observed on the shroud top surface. However, the qualitative heat transfer pattern was predicted well compared with measurements.

The “frozen rotor” investigations indicate that the film cooling effectiveness was quite sensitive to rotor-stator positions. The steady-state stage calculation seemed to make a good synthesis of the several positions and would likely result in a time-averaged unsteady simulation.

### ACKNOWLEDGEMENTS

This research was performed within the European research project “Aerothermal Investigation on Turbine Endwalls and Blades” (AITEB-2, 6FP, AST4-CT-2005-516113). The permission for the publication is gratefully acknowledged by the authors.

### REFERENCES

- [1] Porreca, L., Behr, T., Schlienger, J., Kalfas, A. I. and Abhari R. S., “Fluid Dynamics and Performance of Partially and Fully Shrouded Axial Turbines“, ASME Turbo Expo, GT-2004-53869.
- [2] Lampart P., Yershov, S. and Szymaniak, M., “Tip Leakage/Main Flow Interactions in Multi Stage HP Turbines With Short-Height Blading“, ASME Turbo Expo, GT-2004-53882.
- [3] Nirmalan, V. and Bailey, J., “Experimental Investigation of Aerodynamic Losses of Different Shapes of a Shrouded Blade Tip Section“, ASME Turbo Expo, GT-2005-68903.
- [4] Giboni, A., Menter, J. and Breisig, V., “Interaction of Labyrinth Seal Leakage Flow and Main Flow in an Axial Turbine“, ASME Turbo Expo, GT-2003-38722.
- [5] Bohn, D., Ren, J. and Tümmers, C., “Unsteady 3D-Numerical Investigation of the Influence of the Shroud Cavities on the Stator-Rotor Interaction in a 2-Stage Turbine“, ISABE 2005-1155.
- [6] Nirmalan, V., Bailey, J. and Braaten, M., “Experimental and Computational Investigation of Heat Transfer Effectiveness and Pressure Distribution of a Shrouded Blade tip Section“, ASME Turbo Expo, GT-2004-53279.
- [7] Haller, B. and Hilditch, M., “External Heat Transfer on a Shrouded HP Gas Turbine Stage“, ASME Turbo Expo, GT-2007-27168.
- [8] Janke, E. and Wolf, T., 2010, “Aerothermal Research for Turbine Components - An Overview of the European AITEB-2 Project“, ASME Turbo Expo, GT-2010-23511.
- [9] Kanjirakkad, V., Thomas, R., Hodson, H., Janke, E., Haselbach, F. and Whitney, C., “Passive Shroud Cooling Concepts for HP Turbines: Experimental Investigations“, ASME Turbo Expo, GT-2006-91250.
- [10] ANSYS CFX, <http://www.ansys.com/products/fluid-dynamics/cfx/>.
- [11] Lehmann, K., Thomas, R., Hodson, H. P., Stefanis, V., 2009, "Heat Transfer and Aerodynamics of Over-Shroud Leakage Flows in a High Pressure Turbine", ASME Turbo Expo, GT2009-59531.
- [12] Lehmann, K., Kanjirakkad, V. P., Hodson, H. P., 2011, "Aerodynamic and Aerothermal Investigation of the Flow around an HPT Rotor Shroud: Heat Transfer and Cooling Effectiveness", to be presented at ASME Turbo Expo, GT2011-45979.
- [13] Lehmann, K., Ph.D Thesis, "Heat Transfer and Aerodynamics of Over-Shroud Leakage Flows in a High Pressure Turbine", Department of Engineering, University of Cambridge, 2009.